IAA-AAS-DyCoSS2-11-02

# A METHOD TO EVALUATE THE PERTURBATION OF NON-SPHERICAL BODIES

**Flaviane C. F. Venditti,[*] Antonio F. B. A. Prado[†]**

The purpose of this work is to show the analysis of a method to measure the amount of perturbation in a trajectory of a spacecraft using the integral of the acceleration over the time. This integral gives the change in the velocity, meaning that, the smaller the change is, the smaller will be the effect of the perturbation. The results are generated for trajectories around oblate and prolate spheroids, representing an irregular body. Because of the non-spherical shape, the trajectory around these bodies will not be like a keplerian orbit. Knowing the change of velocity, it is possible to search for the least perturbed orbits and, consequently, the more stable orbits, which can be very helpful for a space mission.

## INTRODUCTION

The study of perturbations is very important when there are satellites involved. The forces acting on a space vehicle must be known in order to avoid damages or changes in its orbit. For missions where the target is to study small bodies closely, it is important to take into account the gravitational perturbation due to the irregularity of the body. Knowing the perturbations, it is possible to choose the orbits which have less influence on the satellite, for example. Consequently, the corrections due to the perturbations will be smaller in magnitude and frequency. In this work a method to analyze the amount of change in the velocity is applied to irregular bodies.[1] The only perturbation considered here is the gravitational perturbation due to the non-spherical shape of the body.

The Solar System is filled with small bodies, and most of them are located between the orbits of Mars and Jupiter, at the Main Asteroid Belt. A category called NEA, or Near Earth Asteroid, are the ones with orbits passing near the orbit of the Earth.[2, 3] The majority of the asteroids have irregular shapes and are rotating bodies.[4, 5, 6]

## PROBLEM FORMULATION

Many small bodies known have elongated shapes that can be approximated by ellipsoids.[7, 8] The most common form found for the potential in works about asteroids with ellipsoid shapes is

[*] Postdoctoral, Orbital Mechanics and Control Division, INPE, Av dos Astronautas 1758, SJC-SP, Brazil, flaviane.venditti@gmail.com
[†] Researcher, Orbital Mechanics and Control Division, INPE, Av dos Astronautas 1758, SJC-SP, Brazil, antonio.prado@inpe.br

written in terms of spherical harmonics expansion.[9, 10, 11] In this paper this closed form for spheroids will be considered. [12, 13]

Spheroids are figures that have two equal principal axes and one different. The spheroids that will be analyzed here are the prolate and oblate cases, represented in Figure 1.

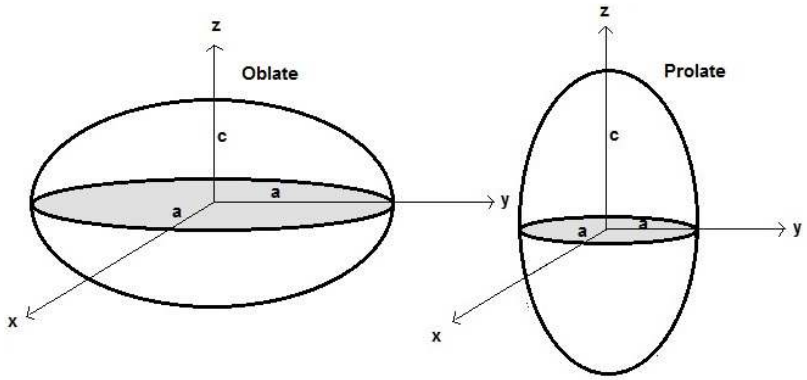


**Figure 1- Oblate and prolate spheroids.**

For the prolate spheroid, the major axis is *c*, and *a* are the two minor axes. The oblate spheroid have two major axes, represented by *a* and, in this case, *c* is the minor axis.

The non-spherical bodies considered in this work can represent well the shape of many minor bodies in the Solar System, if distances not too close from the surface are studied. For cases that require a more precise model, for example when very close proximity to the asteroid is required, it would be recommended choosing another model for the potential.[11, 14, 15] However, the intention of the method that will be presented here is to evaluate for which orbits the perturbation is greater and how fast is the change in the orbital elements due to this perturbation. Thus, the purpose is not to obtain the values of the disturbing forces, but to find families of less perturbed orbits.

The potential of oblate and prolate spheroids are given by Equations (1) and (2), respectively.[12, 13] The difference of the two cases of spheroids is that, for an oblate spheroid $a > c$, and for the prolate spheroid case, $c > a$.

$$V = \frac{a^2 c\sigma\sqrt{c^2+k}\pi(x^2+y^2)}{(a^2-c^2)(a^2+k)} - \frac{2a^2 c\sigma\pi z^2}{(a^2-c^2)\sqrt{c^2+k}} + \frac{2a^2 c\sigma\pi(1-\frac{x^2+y^2-2z^2}{2(a^2-c^2)})\text{ArcSin}[\sqrt{\frac{a^2-c^2}{a^2+k}}]}{\sqrt{a^2-c^2}} \quad (1)$$

Where $a$ and $c$ are the axes, and $\sigma$ the density.

$$V = -\frac{a^2 c\sigma\sqrt{c^2+k}\pi(x^2+y^2)}{(-a^2+c^2)(a^2+k)} + \frac{2a^2 c\sigma\pi z^2}{(-a^2+c^2)\sqrt{c^2+k}} + \frac{2a^2 c\sigma\pi(1+\frac{x^2+y^2-2z^2}{2(-a^2+c^2)})\text{ArcSinh}[\sqrt{\frac{-a^2+c^2}{a^2+k}}]}{\sqrt{-a^2+c^2}} \quad (2)$$

According to MacMillan[13], the term $k$ in the equations for the potential of spheroids satisfies Equation (3).

$$\frac{x^2+y^2}{a^2+k} + \frac{z^2}{c^2+k} = 1 \quad (3)$$

The density can be written as a function of the mass, and is given by Equation (4).

$$\sigma = \frac{3M}{4a^2 c\pi} \tag{4}$$

Where $M$ is the mass, $a$ and $c$ are the axes of the spheroid.

The gravitational potential will be used to obtain the perturbation integral, or *PI*, that can be seen in previous works by Prado.[1, 16] This integral gives the change in the velocity caused by the perturbation, and it depends on the initial conditions established. Therefore, by testing several different configurations for the initial orbits, it is possible to look for the cases where the trajectory is less affected. The integral is given by Equation (5).

$$PI = \int_0^T |Grad(\mathrm{V})|\mathrm{dt} \tag{5}$$

To be able to work with the eccentric anomaly, some arrangements were made. The mean anomaly $M$ is written in two forms, given by Equation (6). The derivative of $M$ in obtained in Equation (7). After some algebraic manipulations, the resulting equation for the perturbation integral, as a function of the eccentric anomaly $E$, can be seen in Equation (9).

$$M = M_o + n(t - t_o) = E - e\sin(E) \tag{6}$$

$$dM = ndt = (1 - ecos(E))dE \tag{7}$$

$$dt = \frac{(1-ecos(E))dE}{n} \tag{8}$$

$$PI = \frac{1}{n}\int_0^{2\pi} |\mathrm{Grad(V)}|(1 - ecos(E))dE \tag{9}$$

Where $n$ is the mean motion, $e$ the eccentricity, *Grad (V)* is the gradient of the potential, and $E$ is the eccentric anomaly.

To calculate the perturbation integral, the partial derivatives are obtained from Equations (1) and (2). The *PI* considers only the disturbing term, so the keplerian term is subtracted from the potential equations before the gradient is calculated. Equations (10), (11), and (12) show, for the oblate spheroid case, the derivatives with respect to $x$, $y$, and $z$, respectively.

$$\frac{\partial V}{\partial x} = \frac{1}{2}GMx\left[\frac{3\sqrt{c^2+k}}{(a^2-c^2)(a^2+k)} + \frac{2}{(x^2+y^2+z^2)^{3/2}} - \frac{3\mathrm{ArcSin}\left(\sqrt{\frac{a^2-c^2}{a^2+k}}\right)}{(a^2-c^2)^{3/2}}\right] \tag{10}$$

$$\frac{\partial V}{\partial y} = \frac{1}{2} GMy \left[ \frac{3\sqrt{c^2+k}}{(a^2-c^2)(a^2+k)} + \frac{2}{(x^2+y^2+z^2)^{3/2}} - \frac{3\text{ArcSin}\left(\sqrt{\frac{a^2-c^2}{a^2+k}}\right)}{(a^2-c^2)^{3/2}} \right] \quad (11)$$

$$\frac{\partial V}{\partial z} = GMz \left[ \frac{3}{(-a^2+c^2)\sqrt{c^2+k}} + \frac{1}{(x^2+y^2+z^2)^{3/2}} + \frac{3\text{ArcSin}\left(\sqrt{\frac{a^2-c^2}{a^2+k}}\right)}{(a^2-c^2)^{3/2}} \right] \quad (12)$$

Where $G$ is the gravitational constant with value of $6.6738 \text{x} 10^{-11}$ $m^3/kg.s^2$.

The same process of obtaining the partial derivatives is made for the case of a prolate spheroid. The results are shown on Equations (13) to (15).

$$\frac{\partial V}{\partial x} = \frac{1}{2} GMx \left[ \frac{3\sqrt{c^2+k}}{(a^2-c^2)(a^2+k)} + \frac{2}{(x^2+y^2+z^2)^{3/2}} + \frac{3\text{ArcSinh}\left(\sqrt{\frac{-a^2+c^2}{a^2+k}}\right)}{(-a^2+c^2)^{3/2}} \right] \quad (13)$$

$$\frac{\partial V}{\partial y} = \frac{1}{2} GMy \left[ \frac{3\sqrt{c^2+k}}{(a^2-c^2)(a^2+k)} + \frac{2}{(x^2+y^2+z^2)^{3/2}} + \frac{3\text{ArcSinh}\left(\sqrt{\frac{-a^2+c^2}{a^2+k}}\right)}{(-a^2+c^2)^{3/2}} \right] \quad (14)$$

$$\frac{\partial V}{\partial z} = GMz \left[ \frac{3}{(-a^2+c^2)\sqrt{c^2+k}} + \frac{1}{(x^2+y^2+z^2)^{3/2}} - \frac{3\text{ArcSinh}\left(\sqrt{\frac{-a^2+c^2}{a^2+k}}\right)}{(-a^2+c^2)^{3/2}} \right] \quad (15)$$

In order to normalize the results, the integral of the partial derivatives, that gives the *PI,* is divided by $2\pi$.

## RESULTS

### Oblate Spheroid

The amount of perturbation over time may now be analyzed calculating the integral of the potential derivatives over a period of time. Several initial configurations can be used to test which one have the least value for the perturbation integral. First it will be shown the results for the case of an oblate spheroid. The initial values used on the following results are: the dimensions of the oblate spheroid is 5 km for the major axes, and 2.5 km for the minor axis; the orbit radius for the oblate and prolate cases is 10 km; the mass considered, also for both cases, is $2 \text{x} 10^{13}$ kg. Figure 2 shows the acceleration as a function of the inclination for one orbital period considering a circular orbit.

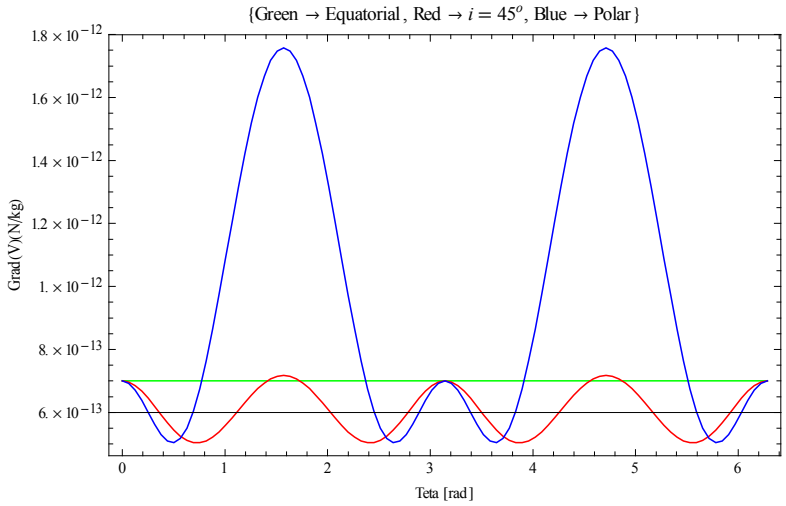


**Figure 2- Acceleration for one revolution for an oblate spheroid.**

The oblate spheroid has two equal major axes, thus the acceleration for an equatorial orbit is constant in every point of the orbit. Figure 2 shows that the variation of the acceleration is much higher for polar orbits. That is because the *c* axis measures half of the length of the major axes, so when it passes closer to the body, the acceleration grows, and decreases after leaving these nearest locations. Therefore, the inclination of $90^o$ is the situation in which the acceleration varies the most.

Using Equation (9), Figure 3 shows the evolution of the perturbation integral, as a function of the inclination for one orbital period, considering a circular orbit.

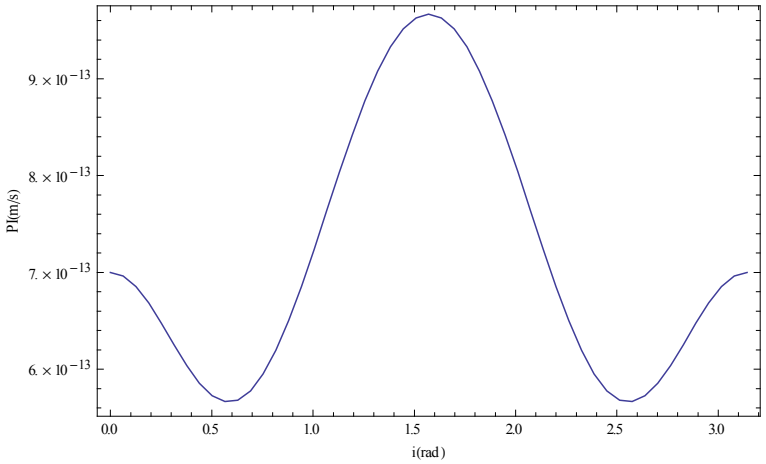


**Figure 3 - Perturbation integral as a function of the inclination for an oblate spheroid in a circular orbit.**

Figure 3 shows that the maximum variation of the *PI* happens when the inclination is $90^o$, which is a polar orbit, and it is where the size of axis suffers more changes during the revolution, confirming what was explained for the acceleration. Next, the perturbation integral will be shown again, now as a function of the inclination, but for elliptic orbits, with several values for the eccentricity.

From Figure 4, that shows five values of eccentricities from zero to 0.4, it can be seen that, the more eccentric is the orbit, the lager will the change in the velocity. As the orbit starts being more elliptic, the equatorial orbit begins to have higher values for the *PI*, due to the fact that the oblate spheroid has the major axes in the equatorial plane. Therefore, as the eccentricity increases, the periapsis of the orbit becomes increasingly close to the body, resulting on a higher perturbation in these points.

The distance from the body is also a point to be analyzed. The orbit radius considered until now is 10 km. The results for the perturbation integral for a semi-major axis from 10 km to 25 km can be seen in figure 5 for inclinations of 0, 45°, and 90° , considering a circular orbit.

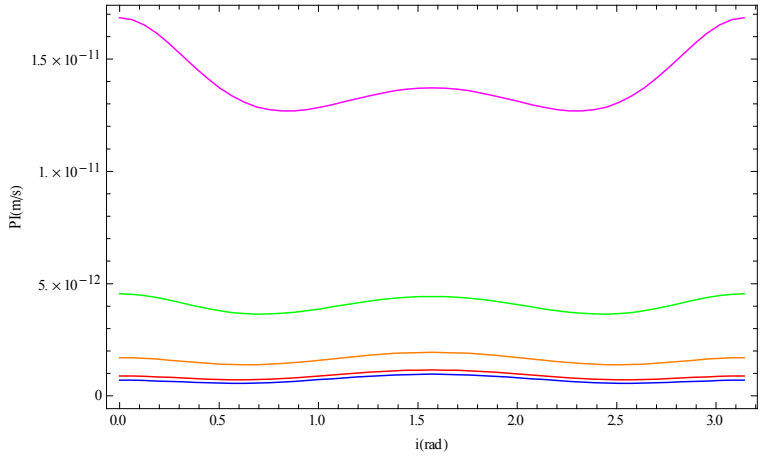


**Figure 4- Perturbation integral versus inclination for an oblate spheroid. Blue, e = 0; Red, e = 0.1; Orange, e = 0.2; Green, e = 0.3; Magenta, e = 0.4.**

The same initial data used in the previous graphic is shown in Figure 6, but also for the case of elliptic orbits. The values for the eccentricity used were: zero, 0.1, 0.2, 0.3 and 0.4.

The effect of different values for the eccentricity can now be seen singly in Figure 7, for an orbit with semi-major axis of 10 km.

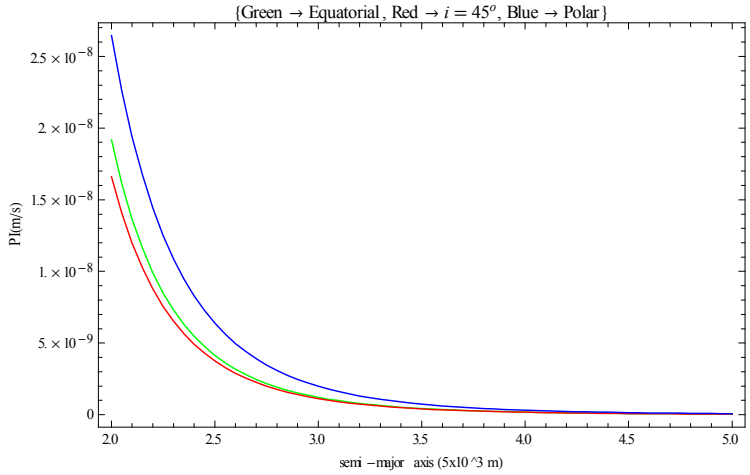


**Figure 5 - Perturbation integral versus semi-major axis for circular orbit, for oblate spheroid.**

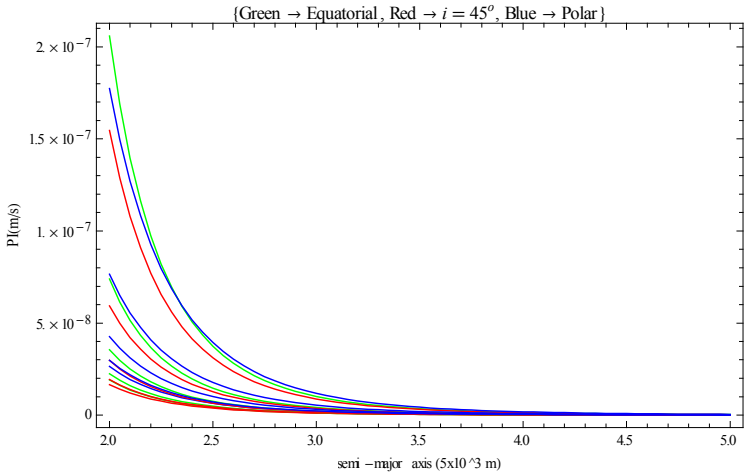


**Figure 6 - Perturbation integral versus semi-major axis for eccentricity from 0 to 0.4. Green is equatorial orbit; Red is for $i$ = 45°; Blue is polar orbit.**

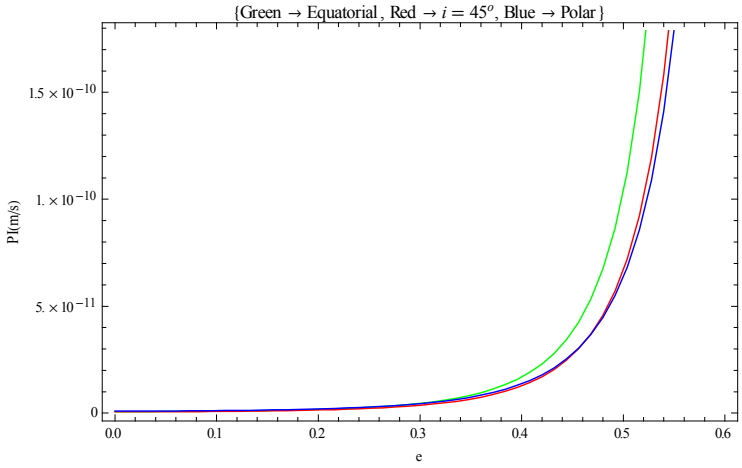


**Figure 7- Perturbation as a function of eccentricity for $i$= 0, $i$= 45°, and $i$= 90°.**

The eccentricity affects practically the same for orbits with inclinations of 0, 45°, and 90°, changing slightly faster for the equatorial orbits because of the major axes. Because the major axis is twice the size of the minor axis, as the eccentricity increases, it may reach the situation of colliding with the body at the periapsis first for the equatorial plane, as explained before. In all cases, the perturbation integral grows very fast between values of 0.4 and 0.5 of eccentricity, because of the proximity from the body. The increase of the perturbation when getting closer to the body was discussed in the previous results, and is confirmed in Figure 7.

Another test that will be presented is to vary the value of the major axis $a$. Figure 8 shows the *PI* as a function of the major axis with values ranging from 3 km to 7 km.

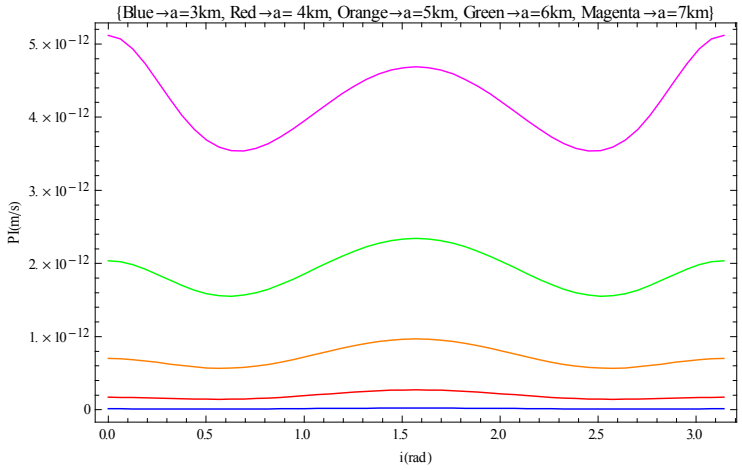


**Figure 8 - Perturbation integral as a function of the inclination for different values for *a* axis.**

When the value for the *a* axis is greater, it differs more from the *c* axis, which measures 2.5 km. In other words, for the chosen parameters, it is when the body is more elongated. For the lowest value of *a*, which is 3 km, the difference from the *c* axis is smaller, getting close to become a sphere. In the case of a homogeneous sphere, the *PI* should suffer no changes for a circular orbit for any inclination, because the gravitational force is the same everywhere around it.

## Prolate Spheroid

Some results will also be presented now for the prolate spheroid. The same values used in the previous results for the mass and orbital radius are used here. The minor axis *a* is considered to measure 2.5 km, and the major axis *c* is 5 km. The acceleration for one revolution is shown in Figure 9 for the prolate spheroid with inclinations of $0^o$, $45^o$, and $90^o$, considering a circular orbit.

Since the two minor axes in the equatorial plane are the same, it is possible to see in Figure 9 that the acceleration is constant. For an inclination of $45^o$ a small variation starts to appear. It is very noticeable that, for polar orbits, the acceleration varies the most. This is because the major axis *c* is twice the length of the minor axes, and for an inclination of $90^o$ the orbit passes by the two extreme values.

Figure 10 shows the perturbation integral as a function of the inclination for the following values of eccentricity: 0, 0.1, 0.2, 0.3, 0.4, and 0.5. As for the oblate spheroid, in equatorial orbits there is no change in the size of the axes, because both axes have equal measurements. Therefore, the change in the velocity is greater for polar orbits. Because the major axis for the prolate spheroid is the *c* axis, which is in the polar plane, even with the increase of the eccentricity, the polar orbits are still the most perturbed cases, different from the oblate spheroid.

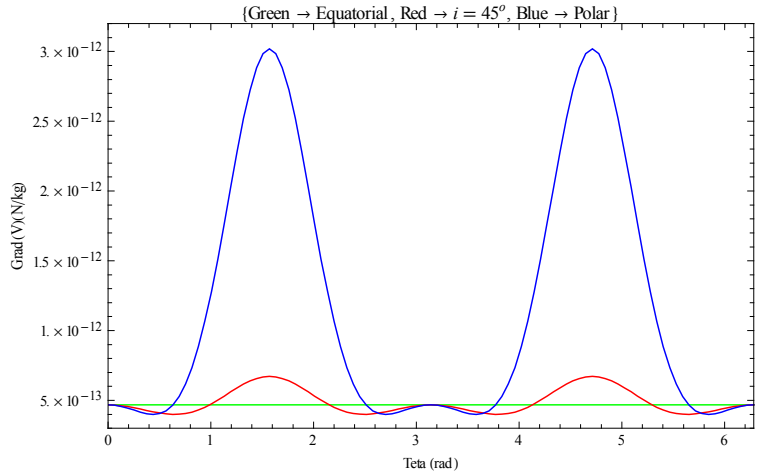


**Figure 9- Acceleration for one revolution for a prolate spheroid.**

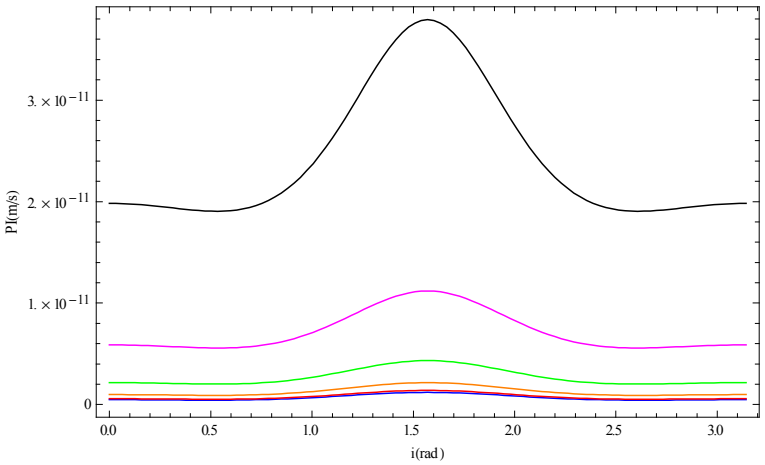


**Figure 10- Perturbation integral versus inclination for a prolate spheroid. Blue, e = 0; Red, e = 0.1; Orange, e = 0.2; Green, e = 0.3; Magenta, e = 0.4; Black, e = 0.5.**

The change in the velocity is greater for very eccentric orbits, and because of the elongated shape of the prolate spheroid, the pattern of the *PI* being higher for polar orbits is the same, just changing the magnitude.

The variation of the orbital radius is studied ranging from 10 km to 25 km, and the *PI* is presented as a function of the semi-major axis for a circular orbit in Figure 11. For closer orbits, it is noticed that, for an inclination of 90°, the perturbation integral shows higher values. For inclinations of zero and 45° the results are practically the same. When the semi-major axis of the orbit increases, which means that it is moving away from the body, the *PI* decreases. This is consistent with the fact that, the closer from an irregular body, the greater will be the effects of the perturbation on an object around it.

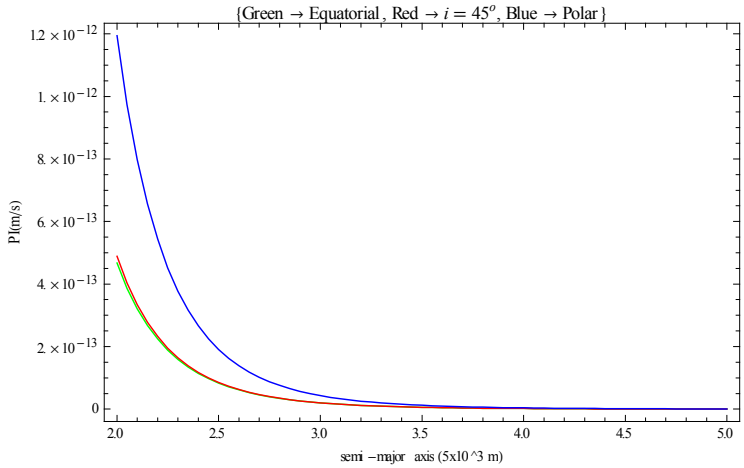


**Figure 11- Perturbation integral versus semi-major axis for circular orbit for a prolate spheroid.**

The next result, in Figure 12, shows the perturbation integral as a function of the eccentricity. The green and red lines, representing the cases for $i = 0$ and $i = 45^{o}$, respectively, are almost superimposed, as it was for the variation in the semi-major axis. The rise of the change in velocity happens faster when the orbit starts getting more eccentric. After eccentricity of 0.4, the *PI* grows rapidly, even faster for polar orbits, because it is getting too close to the body.

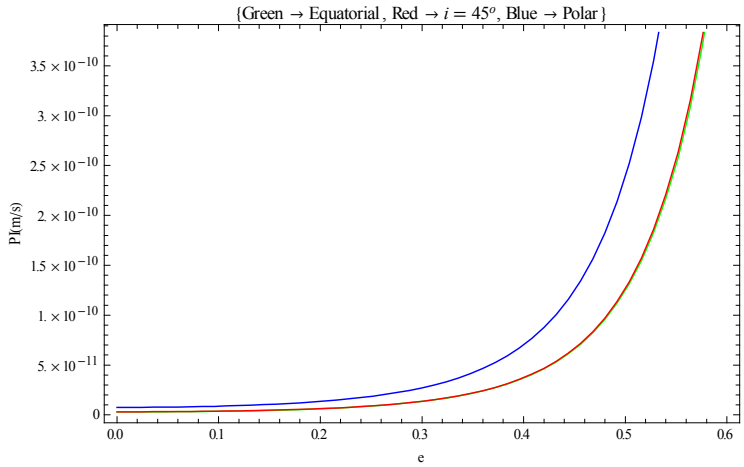


**Figure 12- Perturbation as a function of eccentricity for i = 0, i = 45°, and i = 90°, with a = 10 km.**

Figure 13 considers the variation of the *a* axis, which for the prolate spheroid is the minor axis. The values for *a* goes from 500 m to 4 km. Recalling that, the *c* axis used here measures 5 km.

For smaller values for the minor axis the *PI* has higher values, because the body is more like an ellipsoid. When the value for the minor and major axes are almost the same, represented in magenta color in the figure above, the perturbation is minor, because the shape of the object is approximately like a sphere, as was already explained for the oblate spheroid previously.

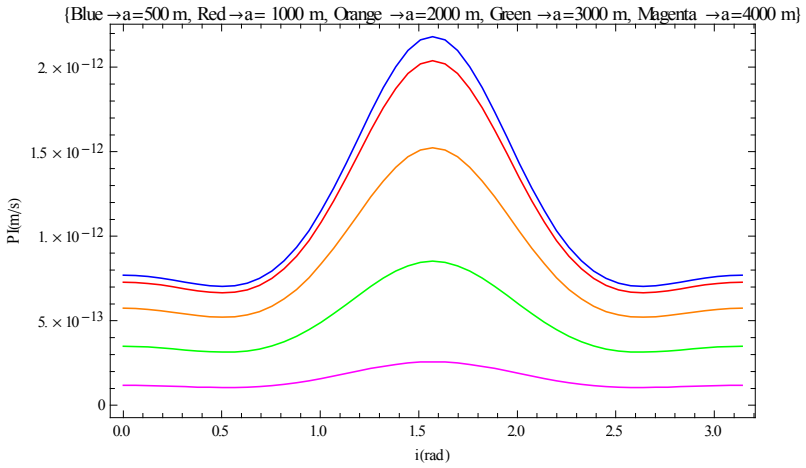


**Figure 13- Perturbation integral as a function of the inclination for a prolate spheroid for different values for *a* axis.**

## Rotation

The results already presented considered an orbit around a fixed body. Using ellipsoids to represent small celestial bodies is a valid approximation in most cases. Asteroids are spinning and some of them quite fast. The rotation of small bodies can be deduced, for example, from light curves.[5, 18, 19] Most of the asteroids are in a principal axis rotation state about the largest moment of inertia, and only a very few are in a different types of rotation, like asteroid Toutatis, that is in a complicated tumbling rotation.[20, 21] Therefore, the results presented here will consider that the spacecraft is in a circular orbit around a rotating celestial body. For the oblate spheroid case, results with rotation in the three axis were obtained. Figure 14 considers rotation in the *z* axis for several rotation periods, denoted by R (R = 0 means no rotation).

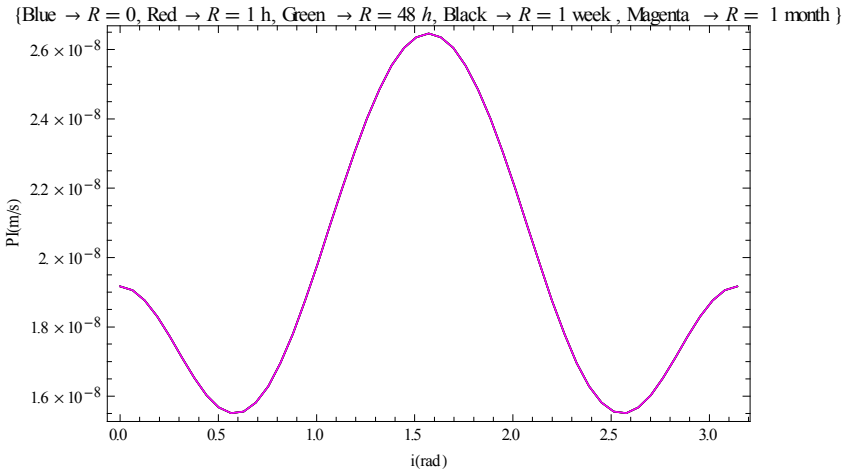


**Figure 14- Perturbation integral versus inclination for different rotation periods in z axis for an oblate spheroid.**

Because of the symmetry of having two equal axes, the rotation for a spheroid in the *z* axis is not affect by the change in the angular velocity. This is true for both spheroids, oblate and prolate. Changing the axis of rotation generates different results. Figure 15 and 16, consider rotation in the *y* and *x* axis, respectively, and show the perturbation integral as a function of the inclination.

In Figure 15 and 16, as the rotation period changes, the difference of the behavior of the curves can be noticed. For the *x* and *y* axes, the case with no rotation, in blue line, and the case of the slowest rotation, in magenta, are very similar. As for the other values of angular velocity, the *PI* varies differently for each particular case. It is clear that the rotation of the celestial body may increase or decrease the total perturbation. In the example shown in Figure 15 the rotation with a period of 48 hours has the minimum average perturbation.

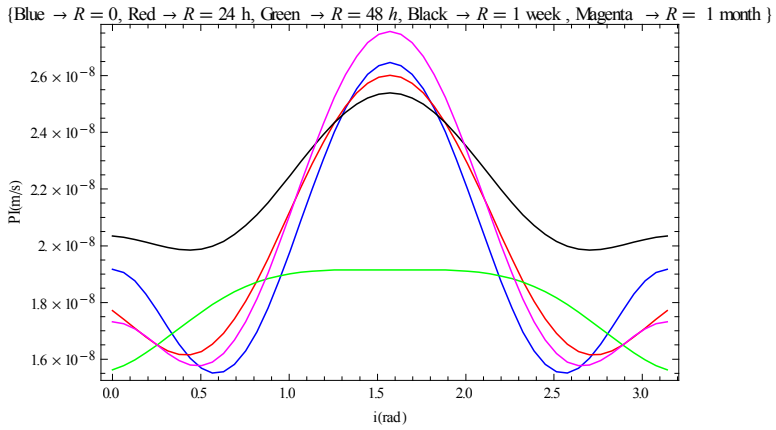


**Figure 15- Perturbation integral versus inclination for different rotation periods in y axis.**

The examples shown above considered a prograde rotation. Considerations for retrograde rotation can also be made. For rotation in any of the axis, the polar orbit tends to have much higher values for the *PI*, which is expected, since the different axis is in the polar plane.

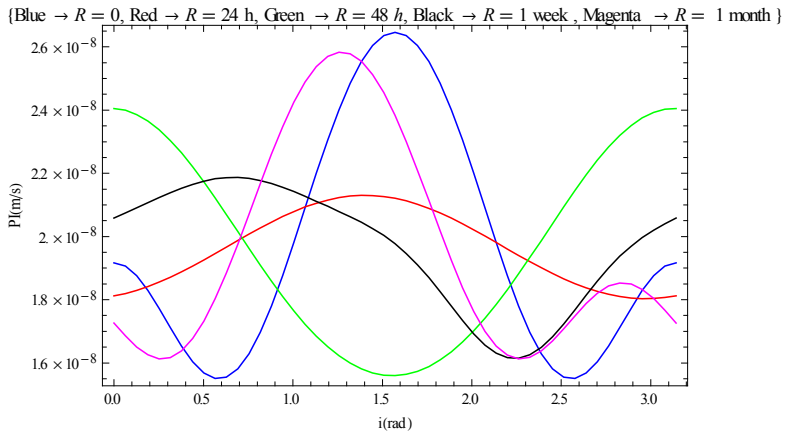


**Figure 16- Perturbation integral versus inclination for different rotation periods in x axis.**

**Lagrange's Planetary Equations**

For bodies that are not point masses, the variations of each orbital element can be obtained using the planetary equations of Lagrange. This set of six differential equations gives the rates of change of the elements considering the disturbing function.[17] Equations 16 to 21 are the six equations.

$$\frac{\mathrm{da}}{dt} = \frac{2}{\mathrm{na}}\frac{\partial V}{\partial \mathrm{M}} \tag{16}$$

$$\frac{\mathrm{de}}{dt} = \frac{1-\mathrm{e}^2}{\mathrm{na}^2 e}\frac{\partial V}{\partial \mathrm{M}} - \frac{\sqrt{1-\mathrm{e}^2}}{\mathrm{na}^2 e}\frac{\partial V}{\partial \omega} \tag{17}$$

$$\frac{\mathrm{di}}{dt} = -\frac{1}{\mathrm{na}^2\sqrt{1-\mathrm{e}^2}\sin i}\frac{\partial V}{\partial \mathrm{o}} + \frac{\cos i}{\mathrm{na}^2\sqrt{1-\mathrm{e}^2}\sin i}\frac{\partial V}{\partial \omega} \tag{18}$$

$$\frac{\mathrm{d}\omega}{dt} = \frac{\sqrt{1-\mathrm{e}^2}}{\mathrm{na}^2\mathrm{e}}\frac{\partial V}{\partial \mathrm{e}} - \frac{\cos i}{\mathrm{na}^2\sqrt{1-\mathrm{e}^2}\sin i}\frac{\partial V}{\partial \mathrm{i}} \tag{19}$$

$$\frac{\mathrm{do}}{dt} = \frac{1}{\mathrm{na}^2\sqrt{1-\mathrm{e}^2}\sin i}\frac{\partial V}{\partial \mathrm{i}} \tag{20}$$

$$\frac{\mathrm{dM}}{dt} = \mathrm{n} - \frac{2}{\mathrm{na}}\frac{\partial V}{\partial \mathrm{a}} - \frac{1-\mathrm{e}^2}{\mathrm{na}^2 e}\frac{\partial V}{\partial \mathrm{e}} \tag{21}$$

Figures 16 to 24 show the results of the integral of the magnitude of the variation of the orbital elements for one period of the spacecraft. The magnitude was used to avoid compensations that leads to near zero integrals, but that still disturbs the orbits. Those plots makes also a mapping that complements the integral approach, and so also help to find orbits that are more stable, by having smaller initial variations rate at the beginning of the orbit. It is clear that there is a good correlation between the curves generated by the integral approach and the variation of the elements.

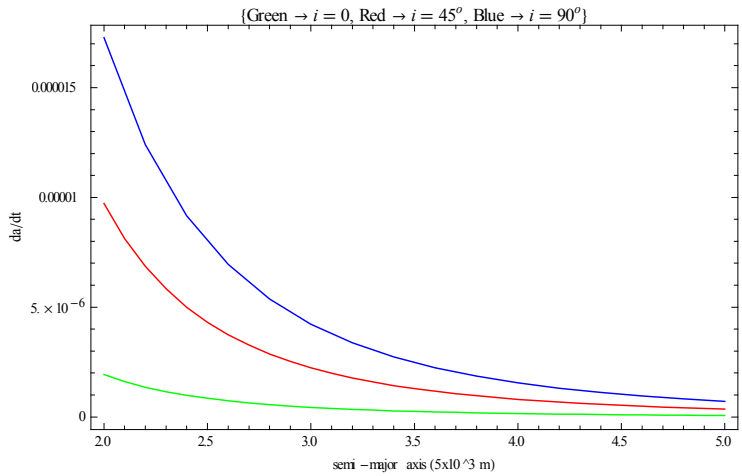


**Figure 16 - da/dt as a function of the semi-major axis for an oblate spheroid.**

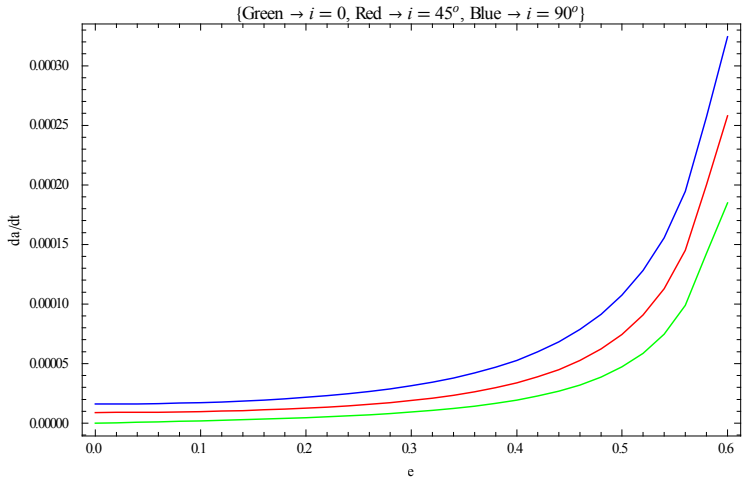


**Figure 17 - da/dt as a function of the eccentricity for an oblate spheroid.**

Figures 16 to 18 show the variation of the semi-major axis as a function of the three orbital elements. The correlation of the graphics with respect to the results obtained for the perturbation integral is very clear, showing that the contribution of this element to the perturbation is higher for smaller values for the semi-major axis.

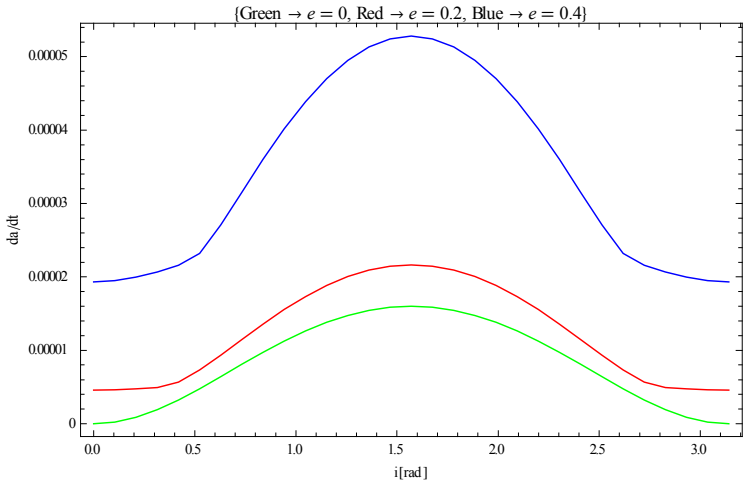


**Figure 18 - da/dt as a function of the inclination for an oblate spheroid, for different eccentricity values.**

Next, using Equation (17), the variation of the eccentricity is presented in Figures 19, 20 and 21. For all the graphics there are three lines, representing different values of inclination, in which green is for equatorial orbits, red for inclination of $45^{o}$, and blue for polar orbits.

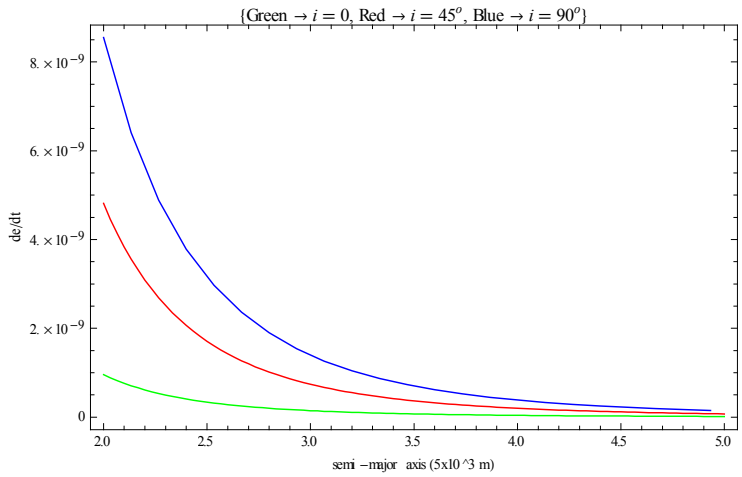


**Figure 19 - de/dt as a function of the semi-major axis for an oblate spheroid.**

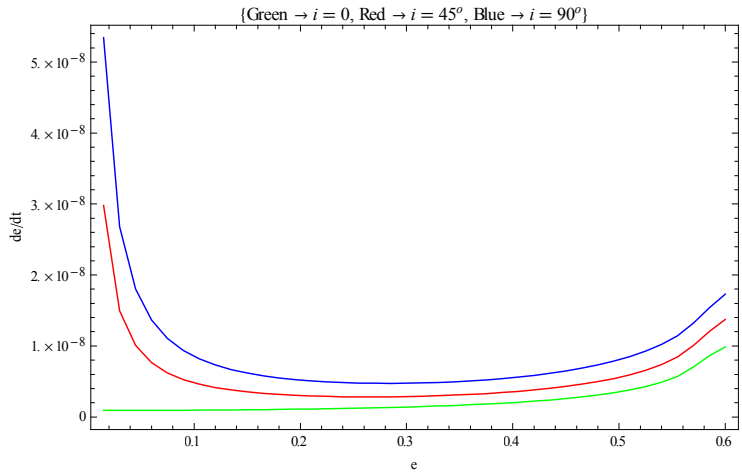


**Figure 20- de/dt as a function of the eccentricity for an oblate spheroid.**

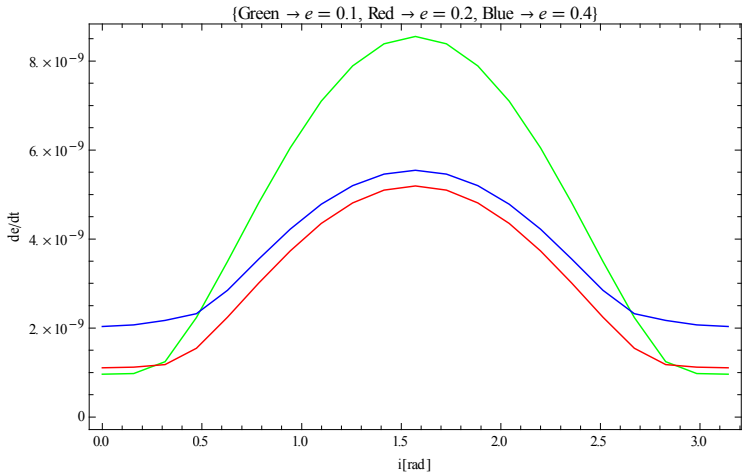


**Figure 21- de/dt as a function of the inclination for an oblate spheroid, for different eccentricity values.**

The following series of graphics that will be shown are for the inclination, obtained from Equation (18). Figures 22 to 24 show the variation of the inclination as a function of the semi-major axis, the eccentricity, and the inclination, respectively.

The results obtained using the Lagrange's planetary equations makes it possible to analyze the effect of each orbital element independently, and therefore, evaluate which element is more affected due to the configuration of the orbit and the object shape.

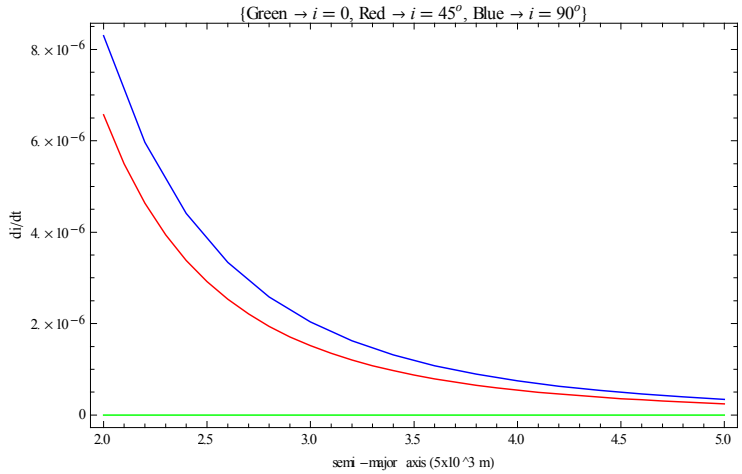


**Figure 22- di/dt as a function of the semi-major axis for an oblate spheroid.**

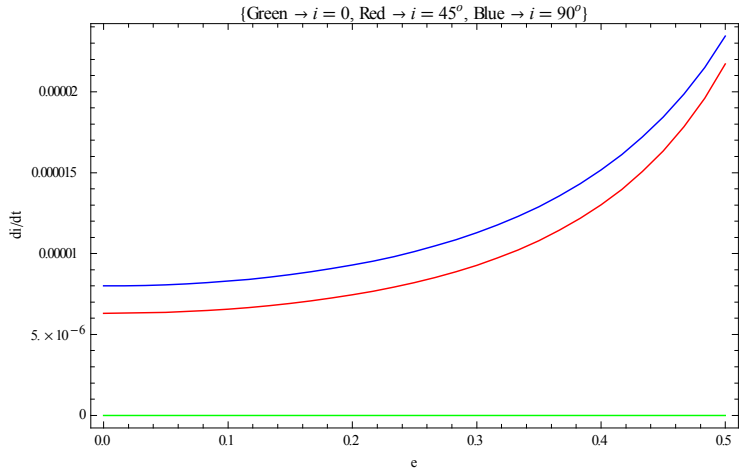


**Figure 23- di/dt as a function of the eccentricity for an oblate spheroid, for different inclinations.**

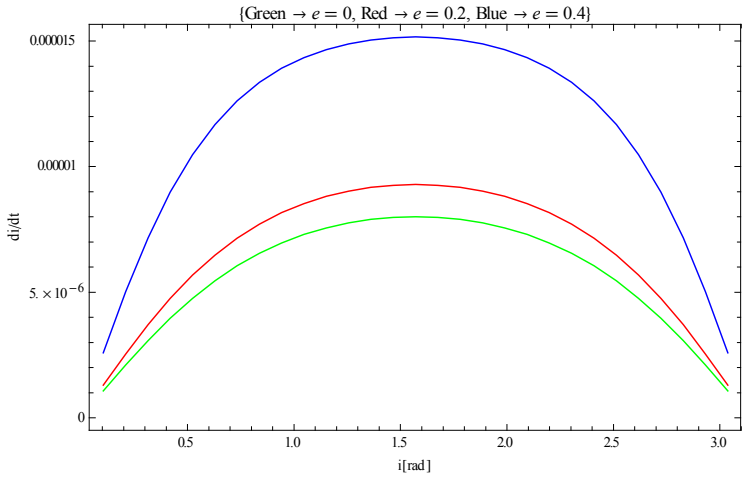


**Figure 24- di/dt as a function of the inclination for an oblate spheroid, for different eccentricities.**

In order to complement the results generated so far, the gravitational acceleration was used to plot trajectories to finalize the analyses. Figure 25 shows, for the oblate spheroid, 200 revolutions for an equatorial orbit, where: image *a* considers a circular orbit and semi-major axis of 10 km; image *b* is for an elliptic orbit (e = 0.3) and same value for the semi-major axis. It is clear the effects of the larger perturbation in the eccentric orbit. Reminding that, the dimensions of the oblate spheroid are 5 km and 2.5 km for the major and minor axis, respectively, and the mass is $2x10^{13}$ kg.

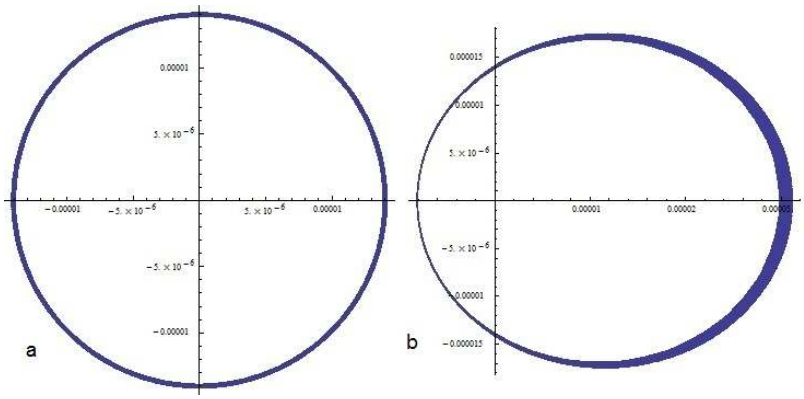


**Figure 25 - Oblate spheroid, i = 0, 200 revolutions, semi-major axis = 10 km. a) e = 0; b) e = 0.3.**

Hereafter, on Figure 26, the configurations are the same as the previous images, except for the inclination, that in this case is 90°. Also, there is image *c* showing the case of a more distant orbit, with semi-major axis of 40 km. It is clear that the effect of the eccentricity is to increase the perturbation, as well as the fact that the polar orbit is more perturbed. The fact that the non-spherical shape perturbs more the orbit when closer to the body is also noticed, proving the results obtained before.

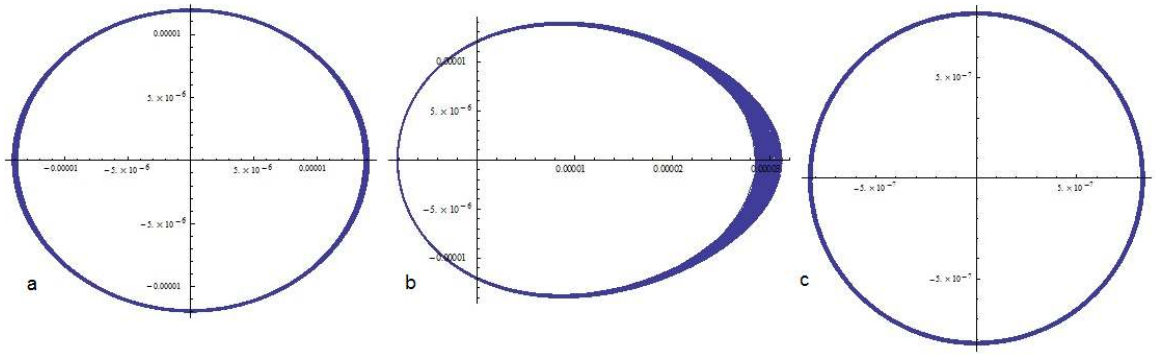


**Figure 26 - Oblate spheroid, i = 90°, 200 revolutions. a) e = 0, semi-major axis = 10 km; b) e = 0.3, semi-major axis = 10 km; c) e = 0, semi-major axis = 40 km.**

The last images represented a body in a fixed position. Figures 27 and 28 consider that the body is rotating, in a circular orbit, with a period of 4 hours, for an equatorial and polar orbit, respectively. In this case it was performed five revolutions around the body. Images *a* consider rotation in the *x* axis, images *b* in the *y* axis, and on images *c* the rotation is in the *z* axis.

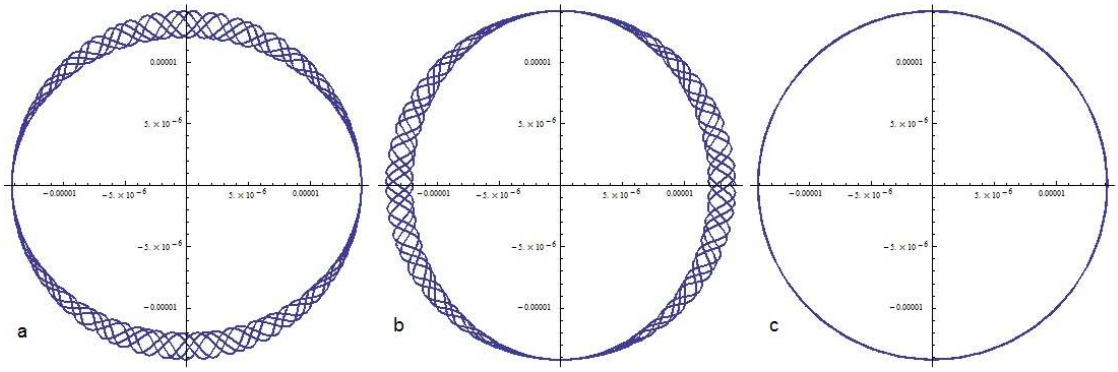


**Figure 27 - Oblate spheroid, e = 0, i = 0, 5 revolutions. a) Rotation in *x* axis; b) rotation in *y* axis; c) rotation in *z* axis**

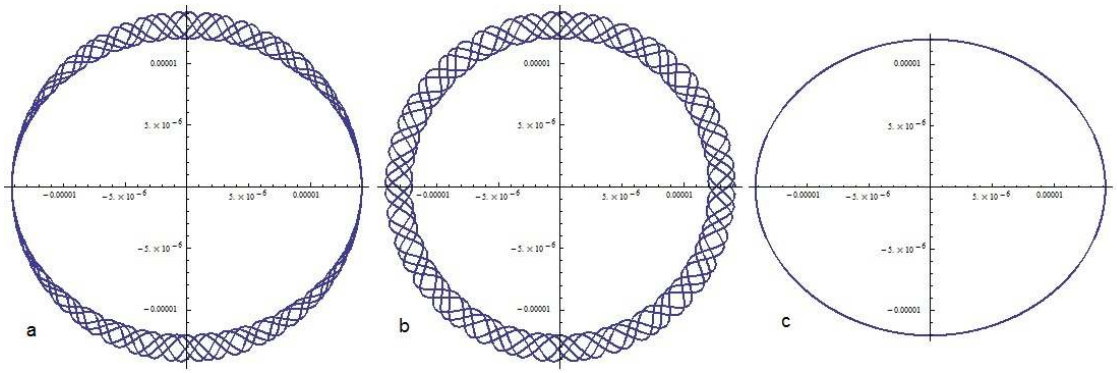


**Figure 28 - Oblate spheroid, e = 0, i = 90°, 5 revolutions. a) Rotation in *x* axis; b) rotation in *y* axis; c) rotation in *z* axis**

These figures illustrate the good correlations between the integral approach, the variations based in the Lagrange´s Planetary equations and the trajectories. They confirm the configurations where the perturbation is greater, obtained with the analyses of the perturbation integral. They also show the importance of considering the right rotation axis of the object, since the intention is to make an analogy to minor bodies of the Solar System, that are rotating irregular shaped bodies.

## CONCLUSION

In this work the study of perturbation of non-spherical bodies is presented. A method of evaluating the amount of perturbation depending on the initial configuration was tested. The formulation of the partial derivatives of the potential of spheroids was obtained using the equations of the potential for the specific cases that were chosen. Some results have been shown for the case of oblate and prolate spheroids. Many cases can be tested changing the initial configurations, and then, the analyses of the cases where the perturbation is smaller can be obtained. Satellites suffer perturbations, changing their initial position, which can be controlled with the use of thrusters. Therefore, knowing the orbits that will have less effect on the satellites is a very import topic for

space mission. An alternative mapping based on the Lagrange Planetary equations were made and shown, with a good correlation with the integral approach. The trajectories plotted also confirmed the results obtained from the other analyses. In this way, the present paper can help mission analyses to choose orbits that are less perturbed to place their satellites.

## ACKNOWLEDGMENTS

The author wishes to thank the financial support from the Brazilian National Council for the Improvement of Higher Education (CAPES).

## REFERENCES

[1]Prado, A. F. B. A; Searching for orbits with minimum fuel consumption for station-keeping maneuvers: an application to lunisolar perturbations, Mathematical Problems in Engineering, 2013.

[2]Scheeres, D. J. Orbital Motion in Strongly Perturbed Environments. Orbital Motion in Strongly Perturbed Environments, by Scheeres, Daniel J. ISBN: 978-3-642-03255-4. Berlin: Springer, 2012.

[3]Bottke, W. F. (Ed.). (2002). Asteroids III. University of Arizona Press, 2002.

[4]Busch, M. W. Shapes and spins of near-earth asteroids. Universal-Publishers, 2010.

[5]Pravec, P. E. T. R., Harris, A. W., & Michalowski, T. Asteroid rotations,.Asteroids III, 113, 2002.

[6]Hudson, R. S., Ostro, S. J. Shape and non-principal axis spin state of asteroid 4179 Toutatis. SCIENCE-NEW YORK THEN WASHINGTON-, 84-84, 1995.

[7]Scheeres, D.J. Dynamics about uniformly rotating triaxial ellipsoids: application to asteroids. Icarus, 121, 67–87, 1994.

[8]Bartczak, P.; Breiter, S.; Jusiel, P. Ellipsoids, material points and material segments. Celestial Mech Dyn Astr, 2006.

[9]Scheeres, D.J., Hu,W. Secular motion in a 2nd degree and order gravity field with no rotation. Celest. Mech. Dynam. Astron. 79, 183–200, 2001.

[10]Kaula, W. M. Theory of satellite geodesy. Waltham, MA: Blaisdell, 1966.

[11]Rossi, A.; Marzari, F.; Farinella, P. Orbital evolution around irregular bodies. Earth Planets and Space, v. 51, n. 11, p. 1173-1180, 1999.

[12]Kellog, O. D.; Foundations of potential theory, Dover Publications. com, 1929.

[13]MacMillan, W. D.; The theory of potential, Dover, 1930.

[14]Werner, R. A. The gravitational potential of a homogeneous polyhedron or don't cut corners. Celestial Mechanics and Dynamical Astronomy, v. 59, n. 3, p. 253-278, 1994.

[15]Geissler, P.; Petit, J.-M.; Durda, D.; Greenberg, R.; Bottke, W.; Nolan, M.; Moore, J. Erosion and ejecta reaccretion on 243 Ida and its moon. Icarus, v.120, n. 1, p.140-157, 1997.

[16]Prado, A. F. B.A. Mapping Orbits Around the Asteroid $2001SN_{263}$. Advances in Space Research, 2014.

[17]Roy, A. E. Orbital motion. CRC Press, 2004.

[18]Torppa, J. Lightcurve inversion for asteroid spins and shapes, 2007.

[19]Kaasalainen, M., Mottola, S., Fulchignoni, M., 2002. Asteroid models from disk-integrated data.In: Bottke, W.F., Cellino, A., Paolicchi, P., Binzel, R.P., (Eds.), Asteroids III, Univ. ofArizona Press, Tucson, pp. 139-150, 2002.

[20]Scheeres, D. J., & Schweickart, R. L. The mechanics of moving asteroids. In 2004 Planetary Defense Conference: Protecting Earth from Asteroids (pp. 23-26).,February, 2004.

[21]Hudson, R. S., & Ostro, S. J. Shape and non-principal axis spin state of asteroid 4179 Toutatis. SCIENCE-NEW YORK THEN WASHINGTON-, 84-84, 1995.